A Related Works

This research proposes a tendon-driven hybrid rigid-soft wearable robot that assists with thumb opposition with an underactuated tendon-driven system. More information will be provided on our website: https://sites.google.com/view/exo-gloveshell. Since the proposed robot focuses on thumb assistance due to the importance of the thumb [1], our review of previous works primarily centers on wearable robots that assist the thumb. [2]

In the pursuit of accurately assisting hand motions, Yun et al. introduced Maestro, a tendon-driven wearable robot that focuses on thumb movements [3]. Maestro assists four degrees of freedom (DOFs) of thumb motions including abduction/adduction of CMC (carpometacarpal) joint and flexion/extension of CMC, MCP (metacarpophalangeal), and IP (interphalangeal) joints, achieved through linkage structures. By employing series elastic components for independent joint torque control, Maestro offers versatility for applying various rehabilitation methods [4]. Another robot, called HX, was specifically developed to concentrate on thumb opposition while utilizing a reduced number of actuators [5]. HX uses a pulley transmission and assists the opposition through the use of two actuators. These robots, characterized by rigid structures for force/torque transmission, are commonly referred to as rigid wearable robots. Rigid wearable robots have shown state-of-the-art performance with precise control; however, these robots are quite large due to their joint alignment mechanism. Consequently, alternative approaches aiming to develop simplified robots have been proposed.

Alternatively, some studies have explored the use of a soft robotic design approach (that composes the robot with soft materials such as a garment or silicone) in wearable robots, because the soft materials allow for a more compact and simplified design of the wearable part due to its advantages in being adapted to the external environment; they are often referred to as "Soft wearable robots." When actuating the soft wearable robots, researchers have used different transmissions (e.g., pneumatic actuation [6, 7], SMA-based actuation [8], twisted tendons[9], and tendon transmission [10, 11]) to fully leverage the benefits provided by soft body. Among these transmissions with their great features [12], we have developed an Exo-Glove shell with tendon transmission capitalizing on its ability to make a safe and compact wearing part.

Soft tendon-driven wearable robots usually focus on assisting finger motions, rather than assisting each joint inside the finger. For instance, most soft tendon-driven wearable robots assist the flexion motion of the index finger with a single actuator, instead of assisting the MCP, PIP, and DIP joints of the index finger independently [13]. Similarly, soft wearable robots, developed to assist the thumb motion, were designed to assist one or two primitive thumb motions. In this paper, we would use the terminology *primitive* instead of *degree of freedom* to express one directional motion of the finger - i.e., we would refer to the flexion of a finger as one primitive motion instead of ambiguous two or three DOF motions. In et al. proposed a robot that made one primitive motion, aimed to assist the thumb flexion/extension [14], while other researchers have developed robots that make two primitive motions consisting of the thumb flexion/extension and thumb abduction/adduction [10, 15–17]; we only count the thumb assistance here to focus on the thumb instead of considering the assistance of other fingers. Since thumb opposition, which is a crucial motion in daily activities, requires both thumb flexion/extension and abduction/adduction, a recent trend has been to assist with two primitive motions.

Although tendon-driven soft wearable robots have received lots of attention due to their simplicity and compactness, these robots have some issues that remain to be solved to enable their widespread use, as explained in the main text. These robots generally require an excessive number of actuators because their tendons can only transmit tensile force. Further, the accuracy of force transmission is often compromised due to deformations of the robot body (details are shown in the Supplementary Video).

In an effort to use fewer actuators, researchers have explored various approaches, including antagonistic actuation [11, 18–20]. These robots actuate one DOF motion with one motor by connecting two wires to a single motor. In these robots, for instance, as the motor rotates in one direction, it winds the flexion wire and unwinds the extension wire, and vice versa for the opposite direction of rotation. It is true that this antagonistic actuation method effectively reduces the number of actuators required in pulley-routed robots [21], however, this approach requires careful consideration of human properties when it is used in a robot that uses suspended tendon routing. This is because the kinematic relationship between the joint angle and the tendon excursion length is not constant in suspended tendon routing - i.e., the tendon Jacobian is a function of the joint angle [22]. Therefore, determining an appropriate radius of the spool at the actuator becomes challenging because the ratio between the excursion length required to flex the joint by a certain angle and the excursion length required to extend the joint by the same amount is not constant; it varies as a function of the joint angle [23]. Moreover, this ratio differs for each individual, necessitating customization.

Another approach to reducing the required number of actuators is to use passive components [10, 15, 24]. Here, the robots assist the flexion through the use of tendons pulled by the actuator and assist extension motions through the use of elastic tendons; these robots store elastic energy for extension motions when assisting flexion motion. Since flexion is more important for most hand motions (flexion requires a higher force to grasp the objects firmly while extension only requires enough force

to make the initial posture), these robots actively assist the flexion motion and passively assist the extension motions. It is true that the use of passive tendons reduces a robot's complexity by using fewer actuators, however, a robot with passive tendons also requires customization, similar to the previous case. This is because the extension torque generated by elastic tendons is determined by the stiffness and elongation of the tendon. When a user has stiff joints, the robot should have a high-stiffness tendon with pretension; however, when a user has joints with low stiffness the robot will make a hyper-extension posture, which is not preferred.

Researchers also have developed the wearable robots using concepts called postural synergy [2, 25, 26] or *under-actuation mechanism* [11, 19] to use less actuators. These two approaches enable researchers to use fewer actuators using similar principles of constraining multiple joints. The difference comes from what they constrain: the postural synergy constrains the position of several tendons by pulling them with a spool (that has several grooves to wind tendons with different radii) while the under-actuation mechanism (i.e., adaptive synergy in [27]) constrains the force applied to the joints. For more information about the actuation characteristics of robots that use postural synergy or under-actuation mechanisms, please read the following paper [27].

Recently, researchers also have developed wearable robots that fall into a gray area, rather than strictly into the category of soft wearable robots or the category of rigid wearable robots. For instance, the SPAR Glove was proposed with the concept of a hybrid wearable robot that has the advantages of both soft and rigid material [28, 29]. Here, a soft glove allows a good fit without any joint alignment mechanism (taking advantage of the benefits of a soft wearable robot) and rigid vertebrae prevent unwanted motion (hyper-extension of joints) to increase safety (to take advantage of the benefits of a rigid wearable robot).

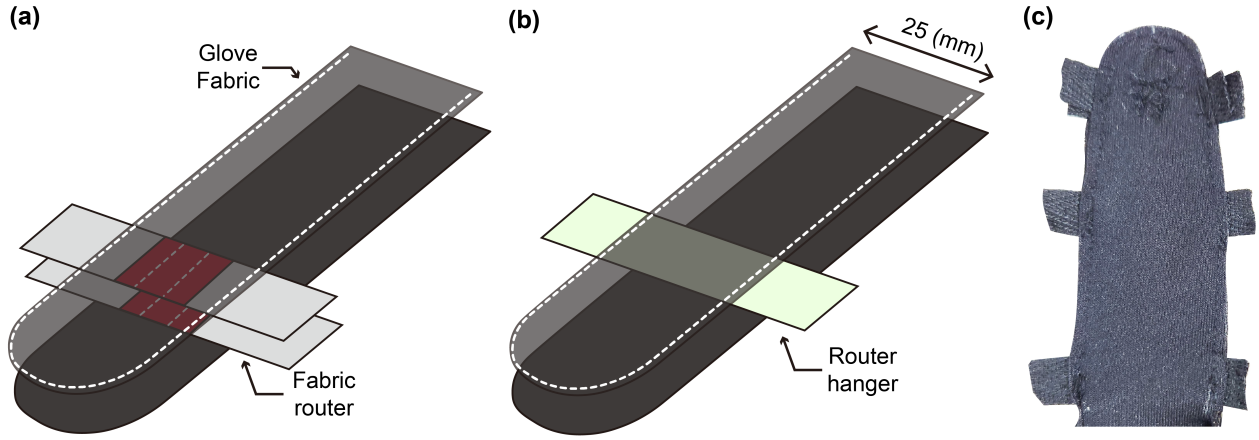

Figure S1: **Fabrication of the wearing part of the proposed and previous robot**
(a) shows the fabrication method used for the wearing part of the previous robot while **(b)** shows the fabrication method used in the proposed robot; white dotted lines in the figure show the seam; **(c)** shows a photo of the inside of the robot's finger part turned inside out.

B Robot Design and Fabrication

B.1 Three-step Fabrication of the Exo-Glove Shell Wearing Part

In the development of the Exo-Glove Shell, the fabrication process of the wearing part was divided into three steps. In this process, we first fabricated the glove part (step 1) and the tendon routers (step 2), respectively. Then, we made the robot by attaching the tendon routers to the glove (step 3). In comparison, previously, the tendon routers were attached to the glove when making the glove itself. Developing the wearing part of the Exo-Glove Shell by dividing it into two parts enabled the robot to be easy to wear (as explained in subsection 2.1 of the main text) and improved the reliability of the actuation (as explained in subsection 2.2 of the main text). This approach also alleviated difficulties in robot fabrication.

Previously, the wearing part of the robot was fabricated as shown in Fig. S1(a). In this fabrication method, we had to sew six layers of fabric (two *fabric tendon routers* that are made of two layers of fabric and two layers of *glove fabric*); since the fabric tendon router was made by sewing two herringbone tapes, the tendon router consists of two layers of fabric. The fabrication of the previous robot's wearing part was difficult because it is difficult to sew six layers of fabric that have only 25mm width at one time. Moreover, it was difficult to align the center of the tendon router with the center line of the glove fabric. This is because – since the *tendon routers* are located between two pieces of the glove garment– we could not see if the *tendon router* was properly positioned. Note that, for a clean seam, the tendon routers are sewn between the glove garment, as shown in Fig. S1(c) because the glove will be turned inside out after the sewing is finished. The fact that sewing is an almost irreversible fabrication method also caused difficulties in the fabrication of the previous robot; for example, if one *fabric router* was misplaced, we had to rebuild the whole robot body, even if the other *fabric routers* were sewn properly.

In Exo-Glove Shell fabrication, however, the metal routers were attached to the glove after finishing the glove fabrication. Therefore, we sew a single layer of *router hanger* (design component that enables us to attach routers to the glove in a compact size) between two *glove fabric* layers, as shown in Fig. S1(b). It was easier to sew the router hanger because, in this approach, we sew only a single layer of fabric. Also, this method was easier since we do not need to consider whether or not the center of the router hanger is well aligned with the center line of the finger. Further, since we attached the *tendon router* after fabricating the robot, it was possible to replace the tendon router without harming other parts of the robot's wearing part.

This three-step fabrication enabled us to modularize the tendon router design based on where the routers are used. Therefore, we have designed three different types of tendon routers that can be used for the index/middle finger (Appendix B.4), thumb metacarpal joint (Appendix B.5), and thumb carpometacarpal joint (Appendix B.6), with each designed for its specific purpose.

This fabrication method also has an advantage in terms of customization because the routers are installed after manufacturing the glove. Therefore, we can easily fit the router to the user after fabricating the glove. This three-step fabrication method (i.e., installation of the router after making the glove) also provides useful maintenance advantages because the modification and replacement of the router are easier. Lastly, the conjunction method of using rivets makes the overall size of the router compact; the overall height of the router is only 3mm, which is sufficient to be used in hand-wearable robots.

B.2 Importance of the router fixation

In tendon-driven SWRs, we usually design the tendon routings of the flexor and extensor to be symmetrical to the center plane—having a normal vector parallel to the target joint axis and passing the center of the joint; see Fig. S2(a) to find a symmetric and asymmetric position of the router. This is because an asymmetric tendon routing applies unwanted directional force to the robot's body possibly causing tendon bias; the tendon bias is a phenomenon (see Supplementary B.3 for detailed analysis) where a tendon and its router slip far from their desired positions as the tendon tension increases. One note here is that, if the tendon bias becomes severe, it reduces the height or changes the sign of the moment arm of the tendon dramatically, which makes it difficult for the robot to assist a user properly. However, even if tendons are routed symmetrically at the fabrication step, the routing can be asymmetric to the center plane due to several unwanted errors such as robot deformation, slippage between the user and the robot, and inaccurate wear. Therefore, for the tendon-driven SWR to be operated properly, it is important to prevent tendon bias, despite initial disturbances or errors.

In soft wearable robots, however, since it is difficult for the soft components (e.g., garment, silicone) to restrain the torsional tilt (due to the robot's softness), it is difficult to prevent tendon bias. Tightly fastening the router to the user could be one option, but this method would increase the pressure applied to the skin, harming the usability. Nevertheless, it is hard to just use rigid structures to prevent tendon bias due to the numerous advantages of the softness of the robot in terms of usability. Therefore, researchers have tried to find suitable compliance of the robot components, according to the location where they are attached [10]. Inspired by this previous research, we developed metal router that prevents the torsional shift of the tendon routing without fastening them to the user. The detailed router design is explained in Appendix B.4 - B.6, and in the next section, we analyze more deeply the reasons for the tendon bias.

B.3 Analysis of the tendon bias phenomena

The tendon bias phenomenon occurs differently in a flexor than in an extensor. For the flexor, the tendon maintains its position or even returns to the desired location (symmetric to the center plane) as the tension of the tendon increases. However, if the extensor tendon is slightly asymmetric to the center plane, the tendon, and its routers often slide further and diverge from the initial location as the tension increases. Sliding occurs more frequently when the moment arm of the extensor is low and the stiffness of the joint is high—where the energy required to extend the finger is larger than the energy required to rotate the router. The tendon bias phenomenon can be explained using slip torque (τ_s in Fig S2) applied to each router. Slip torque is the torque generated from the tendon and applied to the router along the tangential direction of the phalange. The magnitude and direction of the slip torque are the important parameters that determine the occurrence of tendon bias. The direction of the slip torque determines whether tendon bias could occur: In this analysis, if the direction of the slip torque is the same as the direction where the router needs to slide to return to the desired position ($\tau_s < 0$ in this section), this tendon path would recover—or at least maintain—its router position when the tension increases. However, if the direction of the slip torque is opposite to the desired router position's direction ($\tau_s > 0$ in this section), this tendon path could diverge unless some additional torque resists the slip torque. The magnitude of the slip torque determines the vulnerability of the tendon bias: for two router designs with a negative slip torque, the one with the larger slip torque magnitude is prone to diverge from its desired tendon router location.

To calculate the slip torque in the flexor and extensor, we conducted simulations at various joint angles and slip angles in the MuJoCo environment [30]. The slip angle is the discrepancy angle of the router from the center (Fig S2(a)). The phalanges are assumed as capsules with a circular cross-section and the joint is assumed as a sphere. The geometric parameters of each phalange and joint are derived from the anthropometric data near the proximal interphalangeal joints of the index finger in subject 1 ($D_1 = D_2 = 2r_j = 17mm$). The router attaches to the center plane of the phalange and the location of the router is derived from the Exo-Glove Shell ($b_{e1} = b_{f1} = 9mm, b_{e2} = b_{f2} = 12mm, h_{e1} = h_{e2} = 5mm, h_{f1} = h_{f2} = -5mm$) as shown in Fig S2(b). Here, r_j represents the radius of the joint; D_1 and D_2 represent the diameter of the distal and proximal phalange. b_{e1} and b_{e2} represent the axial distance from the joint center to the extensor router located on the distal and proximal phalange, while h_{e1} and h_{e2} represent the height from the phalange surface to the extension tendon router located on the distal and proximal router. b_{f1}, b_{f2}, h_{f1}, and h_{f2} are similar to b_{f1}, b_{f2}, h_{f1} and h_{f2}, but the tendon that they indicate is the flexion tendon. For the whole simulation, the tension of the tendon is maintained as 1N, and the direction of the slip torque axis is preserved, where the positive slip torque means the divergence of the router.

Fig. S2(c) and (d) show the slip torque of the flexor and extensor. As can be seen from the graph, the flexor tendon routing is stable and returns to the center plane, but the extensor generates a torque that makes the router go far away from the desired position.

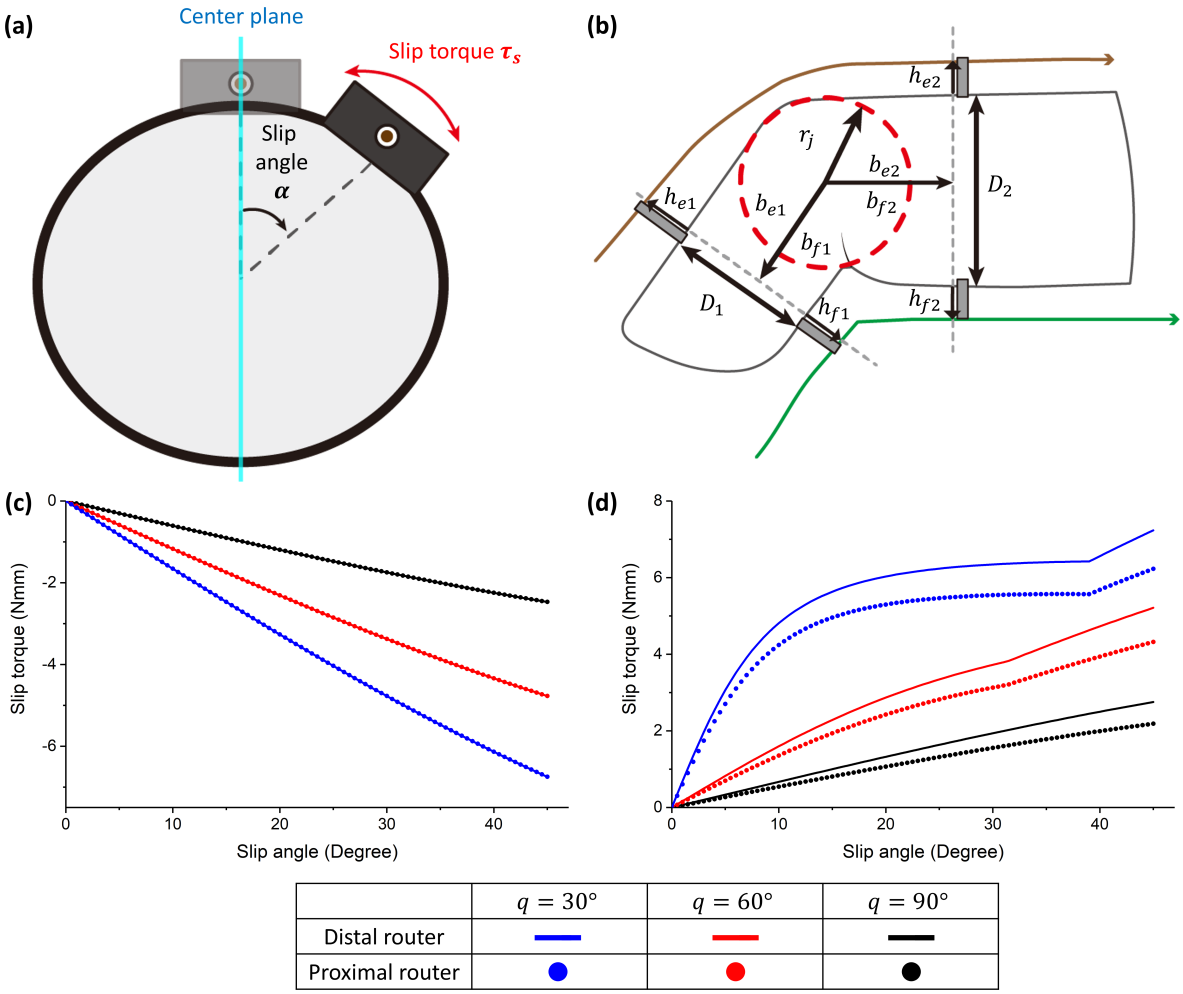

Figure S2: **Analysis of the tendon bias phenomena**
(a) represents a schematic to show the definition of slip torque and slip angle; **(b)** shows geometric parameters used in the MuJoCo simulation; **(c)** and **(d)** show slip torque at the flexor and slip torque at the extensor, respectively.

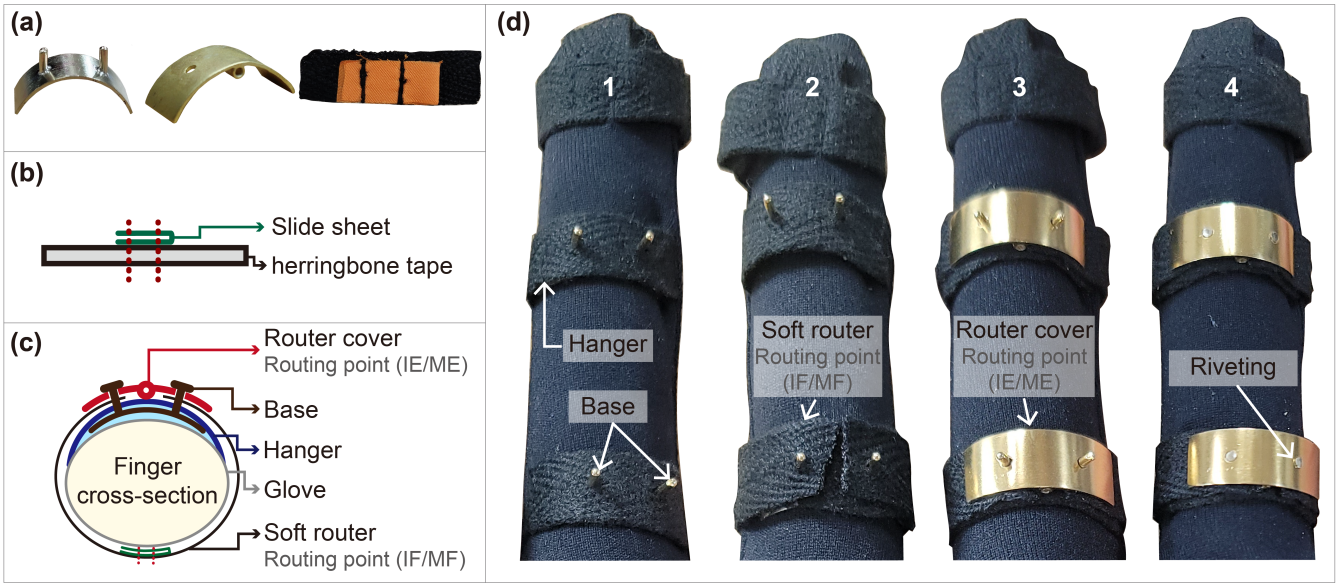

Figure S3: **Overview schematic showing the fabrication and design of the tendon routers for the index and middle finger** **(a)** shows three components (from the left, it shows the router base, router cover, and soft router) that comprise the tendon router for the index and middle finger and **(b)** shows the fabrication method used to make the soft router. The overall schematic that shows the structure of the index/middle router is described in **(c)**; the green line at the soft router in **(c)** describes the slide sheet similar to **(b)**. **(d)** shows the overall process used to attach the index/middle routers to the glove; two horns at the *base* fix both *soft router* and *router cover* through riveting. The slide sheet used in the soft router is orange in **(a)** for visualization, but a black slide sheet was used in the actual robot for aesthetic reasons.

B.4 Router design for the index and middle finger

The Exo-Glove Shell was developed to have four routers at the proximal and middle phalanges of the index/middle fingers. These routers were designed to route two tendons (flexor and extensor) to assist flexion/extension of the index and middle fingers.

When designing the tendon router for the index and middle finger, we first aimed to make it not interfere with other routers on the next finger because the space between the two fingers is narrow. Further, the router was designed to prevent the tendon tilts (which are explained in B.2), for reliable actuation.

To deal with these issues, we designed the index/middle routers with a combination of rigid metal and soft garments. In this design, the rigid metal enables firm fixation, while the soft garment makes the routers not interfere with each other. In more detail, the index/middle router was designed using three parts, as shown in Fig. S3(a): From the left, the router base, router cover, and soft router are shown. Note that the router cover and the base were fabricated by casting. The soft router, on the other hand, was fabricated by sewing the slide sheet to the herringbone tape, as shown in Fig. S3(b); the flexion tendon passes a space inside the overlapped slide sheet. The slide sheet used for the soft router was chosen to reduce the friction applied to the tendon, while the herringbone tape was used to route the tendons – since the herringbone tape is not extensible – without deformation. These three components were attached to the Exo-Glove Shell under the following process; the overall schematic of the index/middle router after installation is shown in Fig. S3(c).

First, the *base* is inserted below the hanger (Fig. S3(d-1)). Then the *soft router* (Fig. S3(d-2)) is pierced into the two cylindrical structures of the base. Finally, by piercing the *router cover* at the two cylinders (Fig. S3(d-3)) and riveting the two cylinders (Fig. S3(d-4)), the installation of router ends. The router cover not only serves to fix the overall router structure, but it also plays a role as a route extensor by including a hole in the top side, as shown in Fig. S3(a) and (c). After installation, the extension tendon was routed to the hole of the *router cover*, while the flexion tendon was routed to the space between the slide sheet of the *soft router*, as shown in Fig. S4(c).

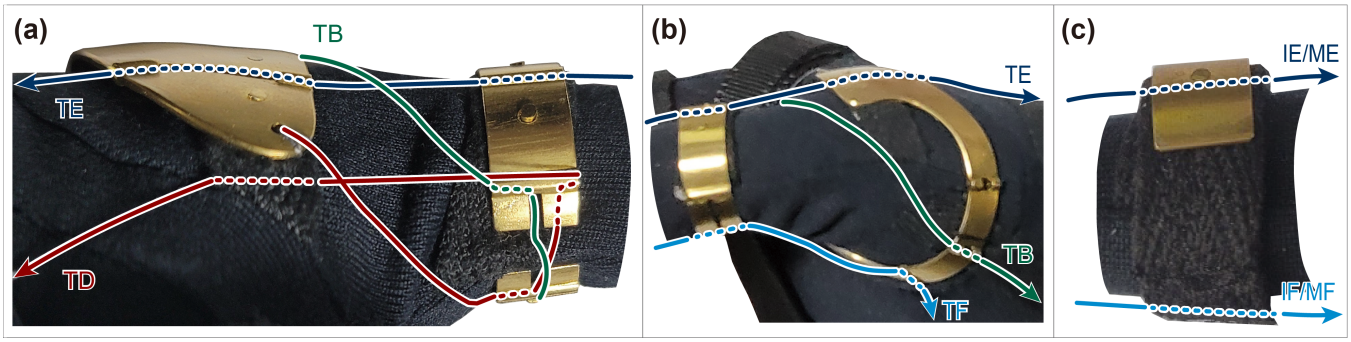

Figure S4: **Tendon routings for the thumb, index, and middle finger**
(a) and **(b)** provide a magnified picture that shows the tendon routing of the thumb routers, while **(c)** shows the routing of the index/middle router. Note that this figure is the same as Fig.2 (f)-(h) of the main text; it is included in the Appendix for the reader's convenience.

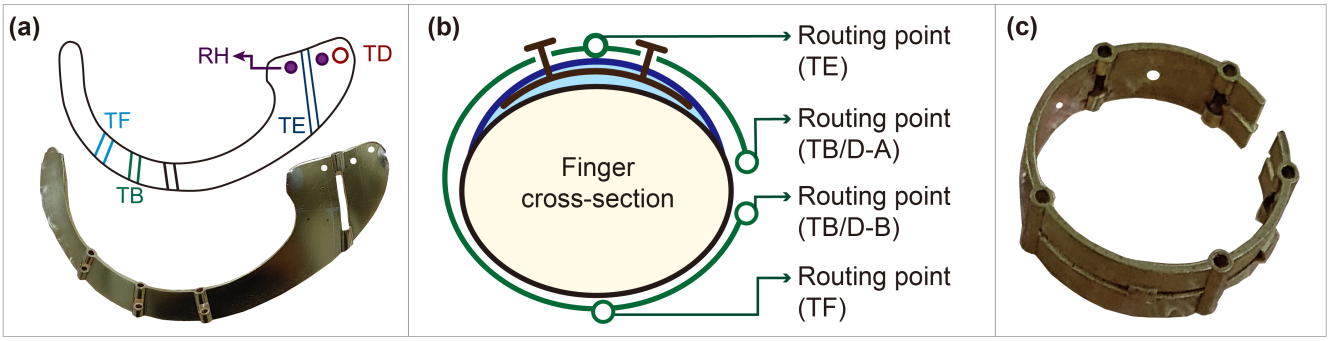

Figure S5: **Overview schematic showing the fabrication and design of the tendon routers for the thumb**
(a) shows the schematic and picture of the thumb CMC router; TE, TB, TD, and TF are the names of the tendons that are expressed in Fig. 1**(g)** of the main text, while the RH means the rivet hole. **(b)** shows the overall schematic of the thumb MCP router, while **(c)** is a picture of the thumb MCP router. TB/D-A and TB/D-B in **(b)** were used to identify the routing points for the thumb abduction/adduction tendons

B.5 Router design for the thumb metacarpal (MCP) joint

The thumb MCP router, a router that fits on the proximal phalange of the thumb, was designed in a ring shape, as shown in Fig. S5(b). Since the thumb is located alone, unlike other fingers, for a firmer fixation, we designed the router with a metal ring (shown in Fig. S5(c)) instead of the combination of a metal shell (shown in the middle of the Fig. S3(a)) and a soft router (shown in the right side of the Fig. S3(a)).

The thumb MCP router routes four tendons (i.e., flexor (TF), extensor (TE), abductor (TB), and adductor (TD)) to make 2 DOF motions, including the thumb opposition. One interesting point about the thumb opposition is that it is a 2.5 DOF motion that consists of flexion/extension, abduction/adduction, and passive internal/external rotation; 'passive' means that internal/external rotation is coupled with other motions [31]. Accordingly, we aimed the abductor/adductor to make the internal rotation for a more natural posture - i.e., the abductor/adductor was routed to assist the coupled motion of internal/external rotation and abduction/adduction. The results of experiment 3 (Fig. 7(a) and (b) in the main text) show that the Exo-Glove Shell successfully assists the coupled motion. In this experiment, the reduction of the thumb orientation means internal rotation.

When pulling the abductor/adductor, since the routings are designed to make internal/external rotation, the router should be fixed more firmly to the user's body; in this case, the router can rotate along with the finger (when the fixation is too weak) because these tendons apply torsion to the router - i.e., the router can rotate in the direction of the blue arrow, which is shown in Fig. 1(c) of the main text. Therefore, it is important to determine the size of the router: if the ring size is too big, the router will not be fixed well to the user, which will induce inaccurate force transmission; alternatively, when the ring size is too small, only some of the users can wear the glove. However, since people have different hand sizes, we cannot decide the ring size before meeting the user. Therefore, we designed the thumb router to have a small slit for easy size adjustment, as shown in Fig. S5(b) and (c); the slit means the space between the routing point (TB/D-A) and the routing point (TB/D-B) in the figure. Interestingly, since the ring was fabricated from brass, the ductility of the metal enabled the router to be fitted well to the user.

Although the slit makes for easy size adjustment, it is important to also think about user comfort. For instance, tight size adjustment can cause discomfort to the user; however, if the router size is set loosely, the router performance will be degraded. For this reason, the abductor and adductor were routed not only to make the motions but also to fasten the router, as shown in Fig. S4(a) and S5(b) - e.g., TB is fixed at the bottom side of the routing point (TB/D-B represented in Fig. S5(b)) and passes through the upper side of the routing point (TB/D-A represented in Fig. S5(b)), as shown in Fig. S4(a). The TD also passes two routing points (TB/D-A and TB/D-B) of the router for the fastening function. With this routing method, it was possible to acquire sufficient fixation force without causing discomfort to the user.

For the flexor and extensor, the tendon routing was designed more simply. In this case, these two tendons were routed through the two holes at the top and bottom of the router, respectively, as shown in Fig. S4(b) and Fig. S5(b). The routing that can not only make motions but also fasten the router (e.g., the routing used in the abductor/adductor) was not used in the flexor/extensor case because these tendons worked well without the fixation function.

B.6 Router design for the thumb carpometacarpal (CMC) joint

The CMC router was designed quite differently, as compared to the other routers. A different approach was chosen because the ring-type structure is difficult to wear on the metacarpal phalange due to the first dorsal interosseous. For this reason, the CMC router was designed in a 'C' shape, as shown in Fig. S5(a); the CMC router has a similar structure to the CMC sleeve used in FLEXotendon [15]. This router was also installed on the glove by the riveting method, through the use of two rivet holes (RH in Fig. S5(a)), similar to the other routers.

The main role of this CMC router is to stabilize the tendon path. When the CMC router does not exist, the tendons tend to make the shortest path between the wrist and the MCP router, causing the Bowstring phenomenon. Therefore the CMC router was designed to prevent the above-mentioned phenomenon by routing the TF, TB, and TE tendons as shown in Fig. S4.

One concern about the CMC router is that the fixation of the router could be weak compared to other routers due to its geometrical limitations (i.e., C shape due to the first dorsal interosseous). Also, since the shape of the area near the thumb metacarpal phalanges of the thumb varies from person to person, it is difficult to determine a single appropriate shape for all users. However, similar to the case of the MCP router, the metal ductility enabled the router to be fixed well to the user - i.e., after applying the glove, the users can fasten the router to their body by deforming it.

B.7 Actuator design for the under-actuated tendon routing

One of the main contributions of the Exo-Glove Shell is its under-actuated tendon routing that uses fewer actuators. Here, one possible problem is that the overall tendon routing can become complicated when using an under-actuation mechanism.

This is because the tendon should pass through multiple fingers. For this reason, we used a Slider-Tendon linear actuator, developed in previous research [32]. Although the actuator is not different from the Slider-Tendon linear actuator presented in the previous research, it is notable to mention the actuator in this paper because the use of the Slider-Tendon linear actuator alleviates the difficulties in designing the under-actuated tendon routings. Therefore, it was possible to use fewer actuators without complicating the end-effector.

B.8 Robot Fabrication

One of our robot's contributions is its easy fabrication method. When fabricating the glove part, we used a conventional glove pattern which can be easily found on the online website. The only thing we added to the pattern is the lines that can be used to place the herringbone tape (it roles as a router hanger as shown in Fig. S3(b) and (c)). Therefore, anyone who wants to start fabricating the hand-wearable robot can just try fabrication without any experience. In the fabrication, as shown in Table S1, we have made the glove using garments for nylon leggings because it made a good fit and nice wearing feeling to the user. For the low-friction garment, we have used *Slide sheet*, a garment that has been used to transfer the patient, with a thickness of 0.05mm. Herringbone tapes, the ones with a 10mm width, were used.

Table S1: Material list for the robot fabrication

Robot part	**Material**	**Specification**
Glove	Garment for nylon leggings	–
Low-friction garment for the soft router	Slide sheet	Thickness (0.05 mm)
Inextensible garment for the soft router and hanger	Herringbone tape	Width (10mm)
Metal router	Brass	Made by metal casting

It is also notable that we have fabricated the tendon router using metal casting, which is one of the well-used methods to fabricate metal crafts, with brass as a material. We chose brass because it showed the attractive characteristics over other metals. For example, tin and aluminum were ruled out due to their propensity to easily deform in a thin structure; the thickness of the router is only 0.5mm. Titanium, despite its strength, was dismissed due to its high casting cost and lack of ductility. Stainless steel was not used because it was hard to do riveting at room temperature. Pure metals like gold, silver, and copper were avoided due to their poor castability. Also, other plastic materials that could be used to make the structure with 3D printers were not strong enough to prevent the unwanted deformation (which is important as explained in B.2). One drawback of brass, that it is heavier than other metals, was not critical in our case because the router is small enough. The index/middle router weighs only 1.2g, while the heaviest router, the CMC router, weighs 4.51g. Since metal casting allows for scalable production, it was possible to make dozens of basic metal routers (the routers shown in Fig. S3(a)) in the first production stage. Therefore, although the metal casting also requires fabrication time, we could keep developing the robot without a large effort even though we want to try other approaches.

Although the proposed robot does not contain Teflon tubes, components used to reduce the friction between the tendon and the routing points, at the metal routers, the metal router has the advantage of containing Teflon tubes to reduce the friction as shown in Fig. S6. In the previous soft wearable robot fabrication, it was difficult to embed Teflon tubes because we had to put Teflon tubes inside smaller holes (compared to the actual size of the Teflon tubes). However, when we embedded the Teflon tube inside the metal router, even if the hole of the metal router was bigger than the size of the Teflon tube, it was possible to firmly fix the tube by deforming the hole at the metal router with a decent amount of force; thanks to the ductility of the brass, the hole remains its shape even after the applied force is removed.

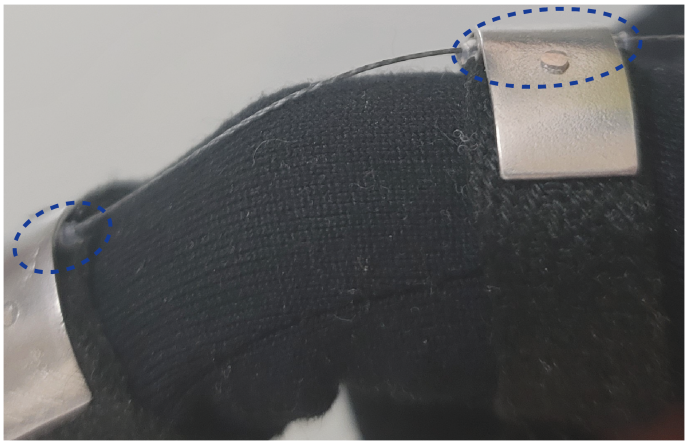

Figure S6: **Teflon tube embedded metal router**
A feature anticipated for inclusion in the next version of our robotic design to reduce the friction at the tendon; the metal router can firmly fix the Teflon tube due to its ductility.

C Approaches to find the appropriate number of actuators

In this research, we aimed to derive the minimum number of actuators required to make three primitive motions (index/middle fingers flexion/extension, thumb abduction/adduction, and thumb flexion/extension) independently by using the under-actuation mechanism. Note that, the under-actuation mechanism is located in the actuator, as described in Appendix B.7; therefore, we only need to think about how the existing tendons should be connected to the actuators without concern for the complexity and the friction issue of the under-actuated tendon routing.

The required number of actuators for the proposed robot system was first derived through the analytical method described in Appendix C.1. However, this approach only provides an initial guess because several assumptions are required for the analytical method that may not be true in the proposed robot system. As an alternative, we also derived a required number of actuators through a simulation, as described in Appendix C.3.

C.1 Analysis to derive the required number of actuators

As a first step to finding the optimal number of actuators, we derived a mathematical expression of the relationship between the joint configuration and the tendon configuration; this relationship is named *tendon Jacobian*, according to previous research [22, 33]. We can define the tendon Jacobian by expressing a kinematic relationship between the tendon and the joint angle as

$$\dot{\mathbf{l}} = \mathbf{J_T}\dot{\mathbf{q}} + \dot{\mathbf{x}}. \tag{S1}$$

where, $\mathbf{l} \in \mathbb{R}^{n_t}$, $\mathbf{J_T} \in \mathbb{R}^{n_t \times n_q}$, $\mathbf{q} \in \mathbb{R}^{n_q}$, and $\mathbf{x} \in \mathbb{R}^{n_t}$ are the tendon length, tendon jacobian, joint angle, and tendon displacement, respectively. n_t and n_q represent the number of tendons and the joints, respectively. Since we are interested in analyzing a method to use fewer actuators, the number of actuators (n_a) might be different from the number of tendons (n_t). Therefore, we also define the relationship between the tendon space and the actuator space. Focusing on the force relationship between two spaces, we would define the relationship between wire tension ($\mathbf{T} \in \mathbb{R}^{n_t}$) and the force input ($\xi \in \mathbb{R}^{n_a}$) of the actuator as

$$\mathbf{T} = \mathbf{U}\xi \tag{S2}$$

with matrix $\mathbf{U} \in \mathbb{R}^{n_t \times n_a}$ that maps the input and the output; physically, this matrix represents how each actuator pulls the tendon with the under-actuation mechanism; the matrix U is similar to the transpose of the transmission matrix (R^T), which is represented in [34]. Using Eq (S2) and the virtual work principle, we can translate the kinematic relationship shown in Eq (S1) into the force relationship between the joint torque ($\tau_a \in \mathbb{R}^{n_q}$) and the actuator force input (ξ) as

$$\begin{aligned}\tau_{\mathbf{a}} &= \mathbf{J_T^T T} \\ &= \mathbf{J_T^T U}\xi \\ &= \mathbf{J_A^T}\xi\end{aligned} \tag{S3}$$

by defining an actuation jacobian ($\mathbf{J_A} \in \mathbb{R}^{n_q \times n_a}$) as $\mathbf{U^T J_T}$. Then, we can analyze the controllability of the tendon-driven system by expressing the generalized inverse form of the above equation as

$$\xi = (\mathbf{J_A^T})^{\dagger}\tau_a + \alpha N(\mathbf{J_A^T}) \tag{S4}$$

where $A^{\dagger}$ and $N(A)$ represent the generalized inverse and the null space of the A matrix, respectively; α represents any arbitrary integer that is used to express the span of the null space. With this equation, if we want the robot to generate the desired joint torque ($\tau_{a,d} \in \mathbb{R}^{n_q}$), we can find an appropriate desired actuation input $\xi_{\mathbf{d}} \in \mathbb{R}^{n_a}$ from the given equation.

One important thing to note here is that the desired actuation input must be positive because the tendon can only transmit tensile force. Therefore, if the desired actuation input from the given equation is negative, we cannot make the desired joint torque even if it satisfies Eq (S4). Interestingly, the solution to find positive actuation input comes from the presence of null space. Suppose we can find any arbitrary positive null vector $N(\mathbf{J_A^T})^*$. In that case, we can always find positive actuation input ξ by summing sufficiently large positive term ($\alpha N(\mathbf{J_A^T})^*$) because we can choose sufficiently large $\alpha \in \mathbb{R}$. In summary, the tendon-driven robot can control the joint torque if the system satisfies the following conditions [22]:

1. The transposed actuation jacobian should have null space.
2. The transposed actuation jacobian should have a positive null vector.

When finding the relationship between joint position output and the actuator position input of the under-actuated tendon-driven robots, researchers have not used the conventional method that represents the kinematic relationship; instead, they have used quasi-static condition (which will be explained in the next paragraph) to represent joint position output from the actuator force input. This is because, in the under-actuated tendon-driven system, the joint angle cannot be defined even if we determine the tendon excursion length - i.e., there exist multiple joint configurations even if the tendon excursion length is defined.

Alternatively, researchers have obtained the joint angle by using the quasi-static condition. Under this condition, similar to the previous study [33], the torque equilibrium equation in the joint domain can be represented as

$$\begin{aligned}d\tau_{\mathbf{total}} &= d\tau_{\mathbf{a}} + d\tau_{\mathbf{c}} + d\tau_{\mathbf{p}} \\ &= d\tau_{\mathbf{a}} + d\tau_{\mathbf{c}} - \mathbf{K}d\mathbf{q} \\ &= 0\end{aligned} \tag{S5}$$

where $K \in \mathbb{R}^{n_q \times n_q}$ is joint stiffness, $\tau_p \in \mathbb{R}^{n_q}$ is a passive torque generated by the passive component at the joint and $\tau_c \in \mathbb{R}^{n_q}$ is torque generated by the external contact wrench; in the wearable robot studies since the human joint has its own joint stiffness, the use of this term is natural.

By rewriting Eq (S5) to represent the joint angle and combining it with Eq (S3), we can obtain the relationship between the joint angle and the actuator force input as

$$\begin{aligned}d\mathbf{q} &= \mathbf{K^{-1}}(d\tau_{\mathbf{a}} + d\tau_{\mathbf{c}}) \\ &= \mathbf{K^{-1}}(\mathbf{J_A^T}d\xi + d\tau_{\mathbf{c}}).\end{aligned} \tag{S6}$$

C.2 Applying the analysis for the proposed system

This subsection explains how previously explained conditions (that determine the joint torque controllability) can be satisfied in the proposed robot system, and whether four actuators are sufficient to assist three primitive motions. The analysis was conducted by simplifying the system as a system that only has three joints ($q_{prim,tabd}$,$q_{prim,tfe}$, and $q_{prim,mfe}$) because we are focusing on primitive motions rather than independent joint motions. With this simplification, we can express joint torque ($\tau_{\mathbf{prim}} \in \mathbb{R}^3$) in primitive angle domain by rewriting the Eq (S3) as

$$\begin{aligned}\boldsymbol{\tau}_{\mathbf{prim}} &= \mathbf{J}_{\mathbf{T}}^{\mathbf{T}}\mathbf{T} \\ &= \mathbf{J}_{\mathbf{T}}^{\mathbf{T}}\mathbf{U}\boldsymbol{\xi}_{\mathbf{6}} \\ &= \mathbf{J}_{\mathbf{A},\mathbf{6}}^{\mathbf{T}}\boldsymbol{\xi}_{\mathbf{6}}\end{aligned} \tag{S7}$$

where $\mathbf{J}_{\mathbf{A},\mathbf{6}} \in \mathbb{R}^{6\times 3}$ and $\boldsymbol{\xi}_{\mathbf{6}} \in \mathbb{R}^6$ are an actuation jacobian and an actuation input matrix specified for the case where six actuators are used. In the tendon routing of our robot, since each tendon controls each direction of three primitive motions respectively, we can imagine Eq (S7) will have a form similar to

$$\begin{bmatrix}\tau_{prim,tabd} \\ \tau_{prim,tfe} \\ \tau_{prim,imfe}\end{bmatrix} = \begin{bmatrix}R_{Tb} & -R_{Td} & 0 & 0 & 0 & 0 \\ 0 & 0 & R_{Tf} & -R_{Te} & 0 & 0 \\ 0 & 0 & 0 & 0 & R_{IMf} & -R_{IMe}\end{bmatrix} \begin{bmatrix}\xi_{6,1} \\ \xi_{6,2} \\ \xi_{6,3} \\ \xi_{6,4} \\ \xi_{6,5} \\ \xi_{6,6}\end{bmatrix} \tag{S8}$$

where $R_* \in \mathbb{R}$ represents an arbitrary variable to express the structure of the transposed actuation jacobian ($\mathbf{J}_{\mathbf{A},\mathbf{6}}{}^T$) and $\xi_{6,*} \in \mathbb{R}$ represents an actuation force input of $*$-th actuator to show the structure of actuation input vector (ξ_6). In Eq (S8), for instance, we can consider $\xi_{6,1}$ and $\xi_{6,2}$ as a tension of the thumb abductor and the thumb adductor, respectively. Similarly, R_{Tb} and R_{Td} can be considered as an instantaneous moment arm of the abductor and adductor; we can also infer that all of R_* will be positive because they represent the instantaneous moment arm; to clarify this argument, we included "$-$" symbol at R_{Td}, R_{Te}, and R_{IMe}. With this interpretation, we can induce that we can adjust the torque ($\tau_{prim,tabd}$) by controlling two variables ($\xi_{6,1}$ and $\xi_{6,2}$).

Now, by considering two conditions of the actuation Jacobian introduced in the previous subsection, we can figure out whether the proposed system with six actuators can control the joint torque of three primitive motions. Using the "symbolic matrix" function from Matlab, we can obtain the null space of the $\mathbf{J}_{\mathbf{A},\mathbf{6}}{}^T$ as below:

$$N(\mathbf{J}_{\mathbf{A},\mathbf{6}}^{\mathbf{T}}) = \begin{bmatrix}\frac{R_{Td}}{R_{Tb}} & 1 & \frac{R_{Te}}{R_{Tf}} & 1 & \frac{R_{IMe}}{R_{IMf}} & 1\end{bmatrix}^T. \tag{S9}$$

Since $\mathbf{J}_{\mathbf{A},\mathbf{6}}{}^T$ has a positive null space vector, we can figure out that the Exo-Glove Shell with six actuators can fully control the three primitive motions.

A similar analysis can be conducted for the case where four actuators are used. Using the actuation input notation (defined in Fig. 1(g) of the main text), the relationship between the joint torque and the actuation input can be represented as

$$\begin{bmatrix}\tau_{prim,tabd} \\ \tau_{prim,tfe} \\ \tau_{prim,imfe}\end{bmatrix} = \begin{bmatrix}0 & -R_{Td} & 0 & R_{Tb} \\ R_{Tf} & -R_{Te} & 0 & 0 \\ R_{IMf} & 0 & -R_{IMe} & 0\end{bmatrix} \begin{bmatrix}\xi_{4,1} \\ \xi_{4,2} \\ \xi_{4,3} \\ \xi_{4,4}\end{bmatrix}. \tag{S10}$$

In this equation, we can infer that each actuation input ($\xi_{4,1}$, $\xi_{4,2}$, $\xi_{4,3}$, and $\xi_{4,4}$) pulls the flexors of the thumb and index/middle finger, thumb adductor/extensor, extensor of the index/middle finger, and thumb abductor, respectively; this is the same order as the actuation input defined in Fig. 1(g) of the main text. Subsequently, by deriving the positive null space vector of $J_{A,4}^T$ as

$$N(\mathbf{J}_{\mathbf{A},\mathbf{4}}^{\mathbf{T}}) = \begin{bmatrix}\frac{R_{Tb}R_{Te}}{R_{Td}R_{Tf}} & \frac{R_{Tb}}{R_{Td}} & \frac{R_{Tb}R_{Te}R_{IMf}}{R_{Td}R_{Tf}R_{IMe}} & 1\end{bmatrix}^T \tag{S11}$$

using Matlab, we can infer that the Exo-Glove Shell with four actuators can fully control three joint torques (represented in the primitive motion domain) as well.

One remaining question might be "Why can't we use fewer than four actuators?". However, in these cases, the transposed actuation jacobian (J_A^T) will not have null space; therefore we cannot always find the positive actuation input under the given desired torque output. In conclusion, we can infer that four actuators are sufficient and minimal to make three primitive motions.

Although previous analysis proves that the minimum number of actuators for our robot might be four, we can use this result only as an initial guess; more actuators may be required in the Exo-Glove Shell because of the simplification used in the analysis. First, J_A is not constant in our system, while the J_A of the previous analysis is regarded as constant. This difference is because, in the previous studies, the tendon is routed via pulleys, so the moment arm of the tendon could be sustained constantly. However, in our system, the tendon is routed via the sheath, so J_T is not a constant; this is usually called *suspended tendon*

routing. In this routing, the Jacobians are functions of the joint configuration, so maybe there could exist some difference. Also, it may not be accurate to simplify joint configurations in primitive joint configuration space. It reduces the dimension from 11 to 3, which could cause any mathematical problem. Therefore, as an alternative method, we found the minimum number of actuators through the simulation, rather than solving it analytically. Details of the simulation are explained in the next subsection.

C.3 Simulation to find the optimal number of actuators

This subsection describes the detailed simulation process we used to find the optimal number of actuators. For the optimization, the objective function was set to maximize the volume of the *opposition workspace*. The opposition workspace is defined as the space where the workspace of the thumb and that of other fingers overlap [35]. This workspace is well used as an indicator to validate the robots that assist or mimic the thumb [36, 37], because thumb opposition is one of the most important functions of the hand in grasping [31]. With this objective function, the simulation was conducted by increasing the number of actuators from one to six. Note that we aimed to apply the under-actuation mechanism between the index and middle finger, so the maximum number of actuators was set to six, instead of eight. This is because the SNU Exo-Glove [14] was an initial design of the proposed robot, and the advantages of using an under-actuation mechanism between the index and middle finger were preserved in the Exo-Glove Shell. Under these conditions, the simulation was conducted using Matlab. The detailed simulation procedure is as follows:

1. Generate the random actuation inputs and divide the actuation input into n steps. A maximum of six inputs are generated because our maximum number of actuators is six.
2. Calculate the initial position of all robot components (i.e. finger, tendon router, tendon) in the Cartesian domain using the forward kinematics.
3. Compute the actuation Jacobian (J_A in Eq (S10)) using the global position of the robot components.
4. Obtain the next step joint configuration using Eq (S10). Further, compute the global positions of the robot components in a manner similar to step 2.
5. Check whether the thumb is overlapped with other fingers. If the thumb overlaps with other fingers, save this position as an opposition workspace. After that, repeat step 3 - step 5, n times.
6. Measure the size of the opposition workspace after the simulation.

In step 1, we used the Monte-Carlo approach to obtain the random actuation inputs since the Jacobians are non-linear; a total of 5,000 random actuation inputs were generated in this step. In detail, we first generated 200 random sets that consist of the initial tension and the final tension. Here, the minimum and maximum values of the initial tension was set to 0 (N) and 0.5 (N), respectively. Similarly, the minimum/maximum value of the final tension was set to 0 (N) and 4 (N). For each initial/final tension set, 25 different tension distributions were obtained. Therefore, a total of 5,000 (200×25) actuation input sets were generated. After that, to solve the forward kinematics, each tension distribution was divided into 1000 steps.

Step 2 calculates the initial global position of all robot components in a global frame (i.e. fixed frame) using the kinematic information of the hand and the tendon router. The kinematic information is summarized in Appendix C.4 and is defined with respect to the body frame (i.e. moving frame). For instance, if the robot component is attached to a certain phalange j, the location of this component is also represented in joint frame j. For this case, the position of the robot component in the global frame can be expressed as

$$\begin{bmatrix} p_{i,b} \\ 1 \end{bmatrix} = T_{bj}(q) P_{i,j} \tag{S12}$$

where, $P_{i,j}$ is a position of a given robot component in the joint frame defined in the Supplementary section C.4, $P_{i,b}$ is a position of a given router in the global frame, and T_{bj} is the translation matrix that maps between the joint frame and the global frame.

Step 3 is a step that calculates a transpose of actuation Jacobian J_A^T using the robot configuration. As can be inferred from Eq (S10), J_A^T can be obtained by multiplying the under-actuation matrix U to the right side of the tendon Jacobian J_T^T as

$$J_A^T = J_T^T U. \tag{S13}$$

Table S2: Hand kinematics

	Metacarpal	Proximal Phalanges	Intermediate Phalanges	Distal Phalanges
Thumb	60.8 (mm)	34.4 (mm)	-	29.0 (mm)
Index	45.0 (mm)	47.6 (mm)	20.1 (mm)	18.7 (mm)
Middle	55.1 (mm)	43.5 (mm)	21.2 (mm)	22.8 (mm)

The tendon Jacobian can be computed using the location of all the robot components obtained in step 2 because this Jacobian is defined via the kinematic relationship between the tendon displacement and joint angle, as shown in Eq (S1).

Using the actuation Jacobian that is obtained in step 3, step 4 calculates the next step joint configuration by using Eq (S10). One important thing to note is that joint stiffness (K in Eq (S10)) is a human property and this value is difficult to define because it is affected by several parameters, such as arm posture, temperature, age, sex, etc. In this study, we used the average value of the previous study, because our study aims to find the optimal number of actuators, rather than to solve the forward kinematics accurately. Further, the position of the robot components in the global frame is calculated using the updated joint configuration, similar to step 2.

In step 5, we checked whether the thumb overlapped with other fingers. When the fingers were overlapped, the overlapped point was included in the opposition workspace. After checking whether the finger configuration was under the opposition workspace or not, the simulation repeats steps 3 to 5 in sequence for 1000 (n in step 1) times.

In the final step, we calculated the size of the opposition workspace using the Matlab functions 'boundary' and 'polyarea', which find the boundary of 2D data sets and measure the size of the boundary, respectively.

Using this simulation process, the values representing the volume of the opposition workspace for each case (i.e., the use of one to six actuators) were obtained. The opposition workspace is visualized in a 2-D plane because the abduction/adduction of the index and middle finger are not considered - i.e., the workspace of the index/middle fingers exists in the 2-D plane, so the overlapped workspace could be visualized in the 2-D plane. Further, for simplification, we added the opposition workspace of the index finger and that of the middle finger for the simulation result.

C.4 Kinematic information of the hand and the tendon routers

This subsection introduces kinematic information about the hand and robot that was used to simulate the Exo-Glove Shell. For the hand kinematics, since the human hand has a complicated structure, we used the simplified hand model proposed in [38]. In this model, for simplification, the thumb Carpo-metacarpal (CMC) joint was divided into three revolute joints to replace the complicated motion of the thumb, as shown in Fig. S7(a). The three DOF motions of the thumb's CMC joints are called abduction/adduction, flexion/extension, and internal rotation (supination/pronation). Similarly, we refer to each divided joint as the CMC_{ABD}, CMC_{FE}, and CMC_{IR} joint, respectively.

The base frame, which is used as a global frame (G.F in Fig. S7(a)) that describes all the motion and torque of the joints, was attached to the orientation of the thumb (i.e, CMC_{ABD} joint). The base frame is defined to have the x-axis as the direction from the wrist to the finger, and the y-axis as the direction from the back of the hand to the palm. Also, each link has its own moving frame (M.F in Fig. S7(a)) that moves along with the links. In the moving frame, the x-axis is defined to be parallel to the bone, and the z-axis is defined to be parallel to the rotation axis of the joint. The z-axis direction was set so that the torque in the flexion, abduction, and internal rotation directions could be positively defined. The definition of the moving frame axis is described in Fig. S7(a). The actual phalange length is expressed in Table S2.

Using the given kinematic hand model, the tendon configuration was derived by defining the location of the tendon routers. Since the location of the tendon routers changes along with the hand configuration, we defined the location of the tendon routers with respect to the moving frame, as described in Table S3. In this table, the X, Y, and Z values in the table are represented in a moving frame coordinate that is attached to a specific finger joint. The I.O in the last column indicates whether the tendon is going into (I) or going out from (O) the router. With this human-robot kinematic information, the model of the Exo-Glove Shell was simulated using Matlab, as shown in Fig. S7(b). The visualization of the hand model was performed using the Syngrasp model [39].

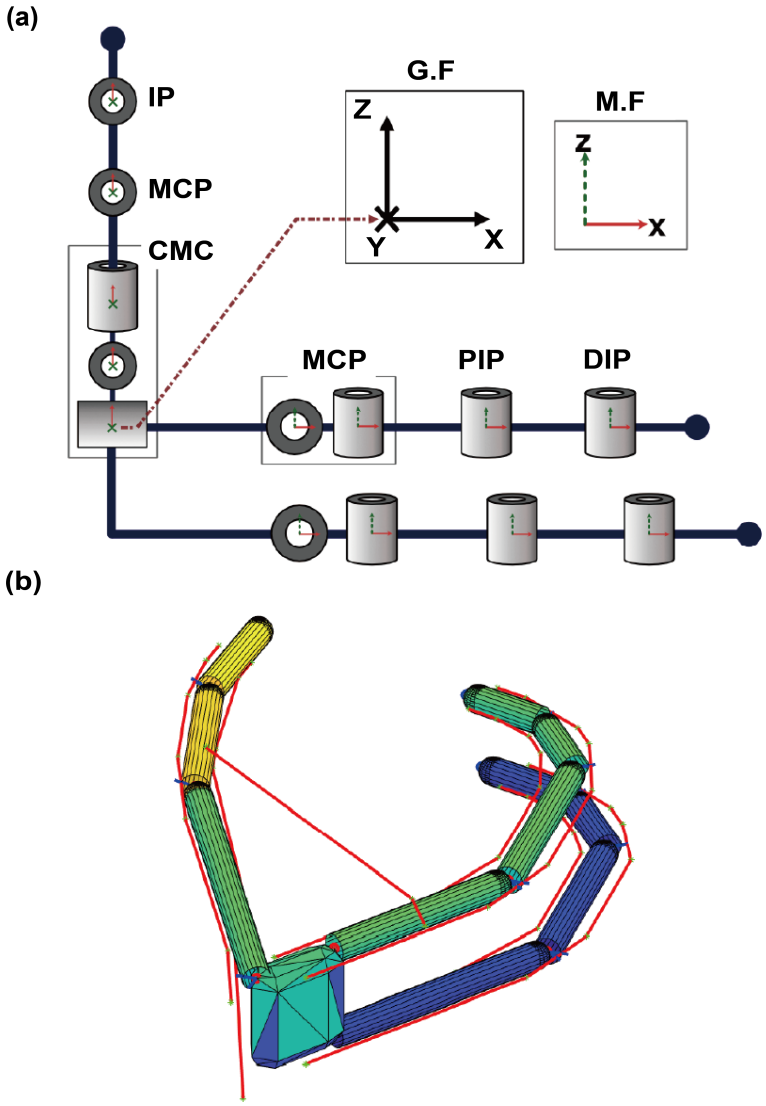

Figure S7: **Overview of the hand kinematics**
(a) shows the simplified human hand kinematic model used in the simulation. The coordinate with the black arrows that is attached at the CMC joint is the global frame (G.F) of the hand. For the moving frames (M.F) that represent the motion of each link, only the X-axis and Z-axis are described for visibility. The moving frames are defined as the right-handed coordinates; the Y-axis can be inferred from the cross product of the Z-axis and X-axis. In the moving frames, the X-axis is defined as a direction parallel to the link and is shown by the red solid arrow. Also, the Z-axis is defined as a direction parallel to the joint rotation axis and is shown by the green dotted arrow. (b) shows the representation of the hand model in Matlab. The red lines in the figure represent the tendons used in the Exo-Glove Shell. Since we only actuate and simulate the thumb, index, and middle finger, the hand model does not consist of either a ring finger or a little finger. Note that, the first bones of each finger are the metacarpal bones, which are located inside the palm of the hand.

Table S3: Position of the tendon router in the finger frame

Tendon1	Finger	Joint	X(mm)	Y(mm)	Z(mm)	I.O	Tendon2	Finger	Joint	X(mm)	Y(mm)	Z(mm)	I.O
	Thumb	IP	5	3	0	O		Thumb	IP	8	-12	0	O
	Thumb	MCP	25	3	0	I		Thumb	MCP	30	-12	0	I
Thumb	Thumb	MCP	5	3	0	O	**Thumb**	Thumb	MCP	8	-12	0	O
Flexor	Thumb	CMC	55	3	0	I	**Extensor**	Thumb	CMC	50	-12	0	I
	Thumb	CMC	8	3	0	O		Thumb	CMC	8	-12	0	O
	Index	Origin	8	4.5	0	I		Index	Origin	-10	-12	0	I
Tendon3	**Finger**	**Joint**	**X(mm)**	**Y(mm)**	**Z(mm)**	**I.O**	**Tendon4**	**Finger**	**Joint**	**X(mm)**	**Y(mm)**	**Z(mm)**	**I.O**
	Thumb	MCP	3	0	4.5	O		Thumb	CMC	8	-6	0	O
Thumb	Thumb	CMC	55	0	4.5	I	**Thumb**	Middle	Origin	40	-10.90	21.38	I
Abductor	Thumb	CMC	40	0	4.5	O	**Adductor**	Middle	Origin	0	-14.11	19.42	O
	Middle	Origin	0	4.5	-20	I		-	-	-	-	-	-
Tendon5	**Finger**	**Joint**	**X(mm)**	**Y(mm)**	**Z(mm)**	**I.O**	**Tendon6**	**Finger**	**Joint**	**X(mm)**	**Y(mm)**	**Z(mm)**	**I.O**
	Index	DIP	8	3	0	O		Index	DIP	8	-12	0	O
	Index	PIP	15	3	0	I		Index	PIP	15	-12	0	I
Index	Index	PIP	8	3	0	O	**Index**	Index	PIP	8	-12	0	O
Flexor	Index	MCP	38	3	0	I	**Extensor**	Index	MCP	40	-12	0	I
	Index	MCP	8	3	0	O		Index	MCP	8	-12	0	O
	Index	Origin	50	3	0	I		Index	Origin	55	-18	0	I
Tendon7	**Finger**	**Joint**	**X(mm)**	**Y(mm)**	**Z(mm)**	**I.O**	**Tendon8**	**Finger**	**Joint**	**X(mm)**	**Y(mm)**	**Z(mm)**	**I.O**
	Middle	DIP	8	3	0	O		Middle	DIP	8	-12	0	O
	Middle	PIP	15	3	0	I		Middle	PIP	15	-12	0	I
Middle	Middle	PIP	8	3	0	O	**Middle**	Middle	PIP	8	-12	0	O
Flexor	Middle	MCP	40	3	0	I	**Extensor**	Middle	MCP	40	-12	0	I
	Middle	MCP	8	3	0	O		Middle	MCP	8	-12	0	O
	Middle	Origin	55	3	0	I		Middle	Origin	65	-12	0	I

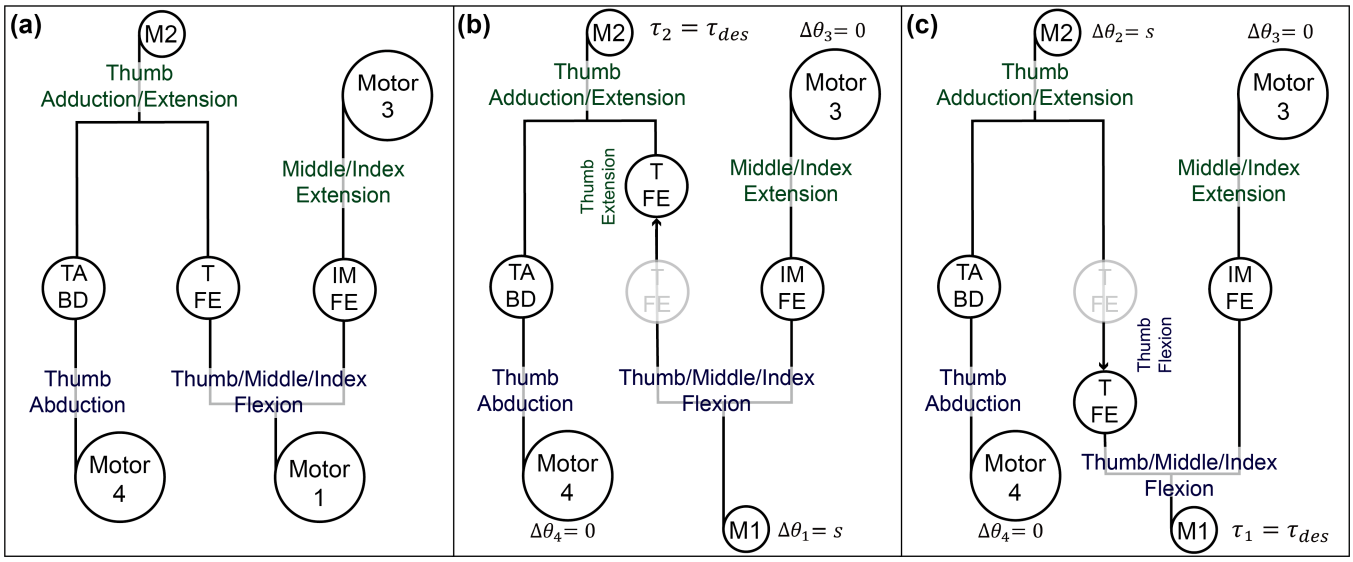

Figure S8: **Simplified schematic how Exo-Glove Shell generates primitive motions**
(a) shows how three primitive motion assistance can be simplified as a schematic; TABD, TFE and IMFE represent Thumb abduction/adduction, Thumb flexion/extension, and Index/Middle fingers' flexion/extension, respectively. **(b)** and **(c)** show how Exo-Glove Shell assists the thumb extension and flexion, respectively.

C.5 Three primitive motions assisted by Exo-Glove Shell

The Exo-Glove Shell assists three primitive motions with only four actuators as shown in Fig. S9 and our supplementary video. Although we have also proven how the Exo-Glove Shell with four actuators can fully control three primitive motions, we believe that providing additional information and the simplified schematic (Fig. S8) could help readers understand how we control our robot to make the primitive motions.

When the robot assists thumb extension as shown in Fig. S8(b), the robot first pulls the thumb abductor using actuator 4 until the tension of the abductor becomes 0.5 (N) and measure that position; the tension is measured using the load cell attached to the actuator and the value 0.5 is decided empirically that makes sufficient tension at the tendon. After that, by controlling this actuator to sustain its position ($\Delta\theta_4 = 0$) in position control mode, we prevented the thumb abduction. Subsequently, by pulling the thumb adduction/extension tendon with actuator 2, the robot can extend the thumb; since actuator 4 is sustaining its position as described previously, the user does not make thumb adduction even if actuator 2 operates. In the meantime, actuator 1 releases the tendon sufficiently ($\Delta\theta_1 = s$) in order not to disturb the thumb extension motion; this is because the thumb flexor can disturb the extension motion if there exists tension at the thumb flexor. The thumb flexion can be assisted similarly to the thumb extension assistance as shown in Fig. S8(c); actuator 1 makes the flexion motion while actuator 3 prevents the flexion of index/middle fingers.

Although the robot generates the motions independently in practice, it is also true that the experimental results (Fig. 7 of the main text) show a small amount of coupled motion. One possible reason for this issue can be a lack of sensors on the glove. For instance, when we think about assisting the thumb flexion motion, the index and middle fingers should not move due to actuator 3. However, due to the tendon elongation, we could find coupled motion even after controlling actuator 3; when the tendon elongates, the fingers can move even if the motor doesn't rotate. This phenomenon could be solved by actively compensating the tendon elongation with external sensors (e.g., bending sensors, external cameras) or by using an elongation model.

The complicated anatomical structure might be another reason for showing the coupled motions. This might be the main reason specifically in thumb abduction motion because actuator 4 only assists thumb abduction; coupled motion should not occur in this direction if the reduced number of actuators is the reason for coupled motion. Although we cannot explain which factors mainly cause the coupled motions, we can say that the coupled motions while assisting thumb abduction are solely affected by the complicated thumb joint structure. Even though we found several reasons for the coupled motion, we decided not to improve the robot to solve these coupled motions because we found that the coupled motions are negligible in practice.

The research that aims to develop robots with fewer actuators can be thought of as the research that tries to find the appropriate dimension of the *workspace*. In general, researchers pursue the dimension of the *workspace* to be the same as the dimension of the *configuration space*. However, since the robot can be complex if the robot has lots of joints, researchers sometimes try to reduce the dimension of the workspace. According to the concept called *postural synergy* [40], we can develop the robot to have the dimension of the workspace as two to make various hand motions. However, in this study, the robot was developed to have a three-dimensional workspace (i.e., the robot was developed to assist three primitive motions). This is because, we thought generating two principal postures (i.e., two principal components of the workspace) accurately is difficult when developing soft hand wearable robots. For example, we should consider the differences in human properties of each person; the elongation of the garment and friction at the tendon also make it difficult to generate accurate posture. Instead, we decided to assist three primitive motions defined in finger level, because it is easier to make even with soft hand wearable robots; the robot can make finger flexion/extension even if the user has different properties.

Regardless of the appropriate dimension of the workspace, our research focused more on answering the other question: how many actuators (in our case, tendon-driven actuators) are required to make the robot cover desired workspace (which is determined as three-dimensional workspace in our case)? This research has verified that, even with non-linearity (e.g., non-linear joint stiffness and non-linear tendon jacobian) in soft hand wearable robot, it is possible to cover 3-dimensional workspace with 4 tendon-driven actuators through analysis (Appendix C.2), simulation (Appendix C.3), and experiment (subsection 4.3 at the main text).

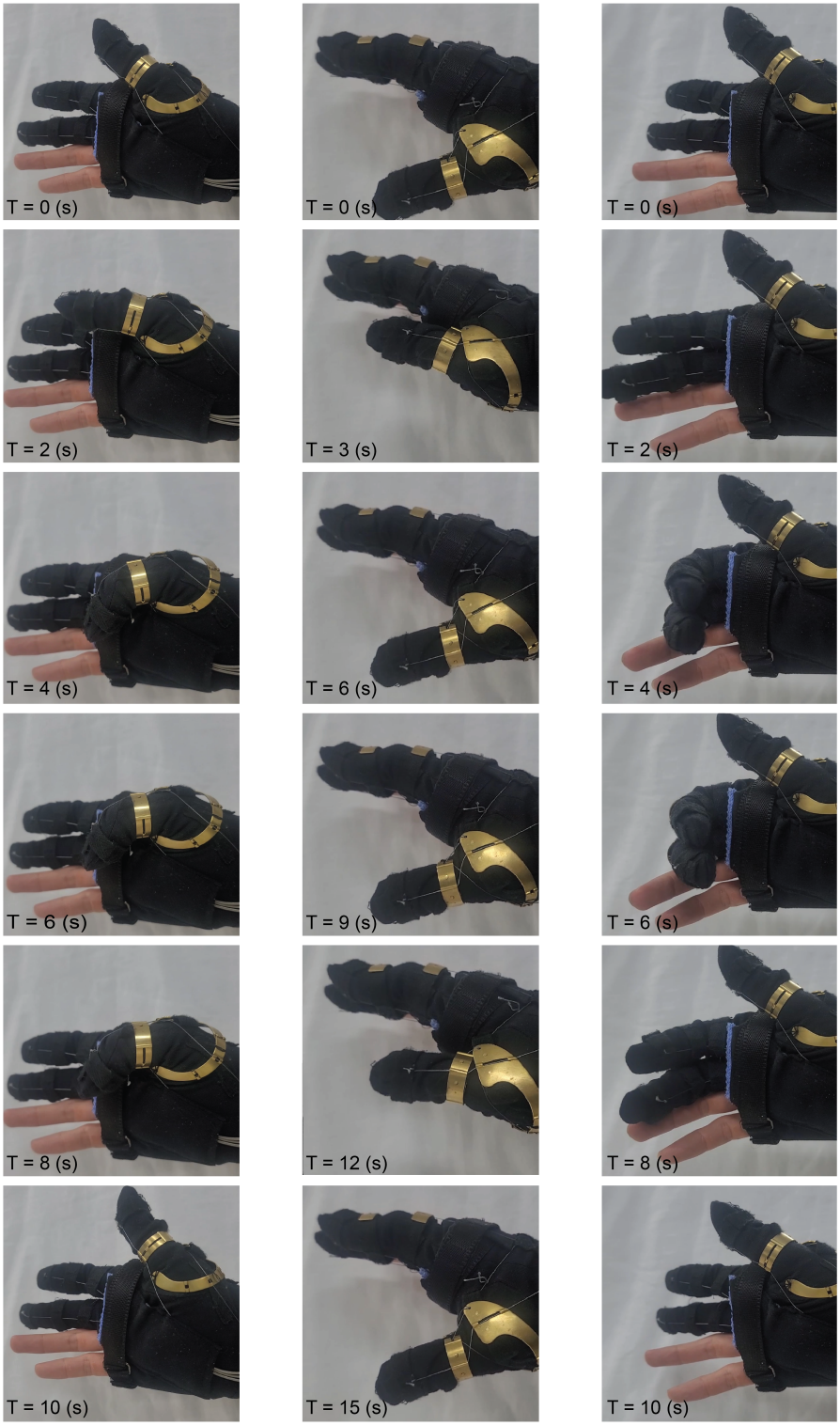

Figure S9: **3 Primitive motions assisted by Exo-Glove Shell**
The first column shows the thumb flexion/extension motion assisted by Exo-Glove Shell; the second column shows the thumb abduction/adduction motion; the last column shows the flexion/extension of the index/middle finger assisted by Exo-Glove Shell. This figure shows the motion changes over time. Check our supplementary video for more information.

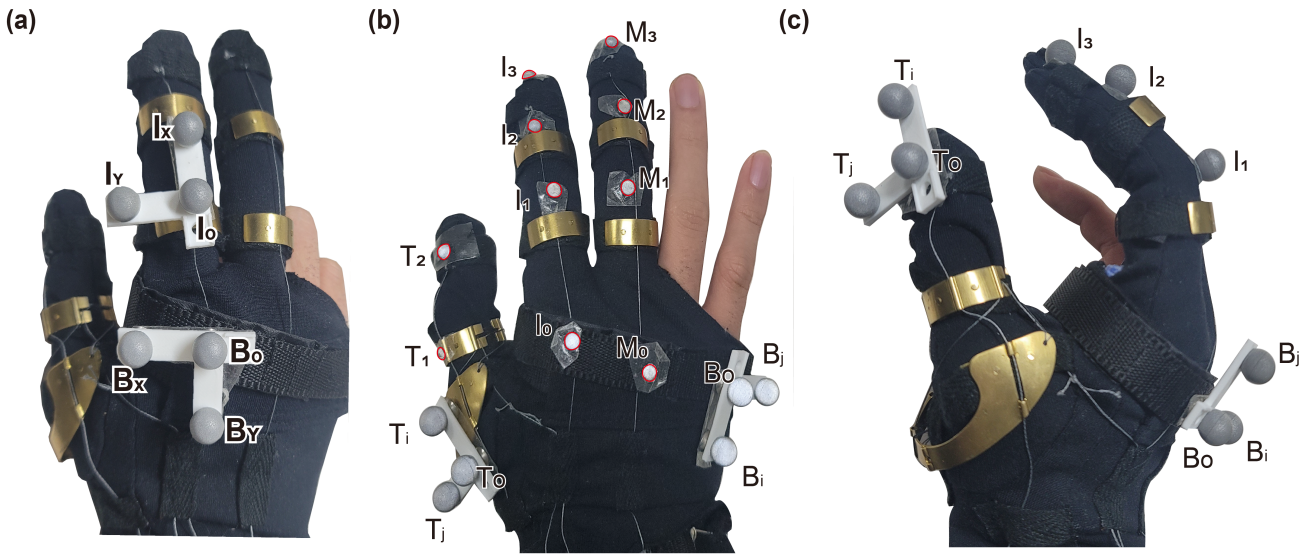

Figure S10: **Marker attachment for experiments 1 - 3**

(a) shows how the markers were attached to measure the rigid router performance (experiment 1 in the main text); **(b)** shows the marker attachment method used to measure joint angles to conduct experiment 2, which is described in the main text. Red borders were drawn to increase the visibility of the markers; **(c)** shows the marker attachment method to measure the position/orientation of the thumb in terms of the index finger configuration used in experiment 3 in the main text.

D Experimental Protocols

D.1 Experimental protocol for experiment 1

Experiment 1 was designed to validate whether or not the use of a metal router enhanced the actuation stability. This experiment was conducted in the following order, examining both the previous robot (Exo-Glove) and the proposed robot (Exo-Glove Shell).

The robot first extended the participant's index/middle finger, set this posture to the initial posture, and then repeated flexion and extension 25 times. During the repeated motions, we measured the position of six markers using the Vicon motion capture system (Fig. S10(a)). Three markers (I_o, I_x, and I_y) were attached at the proximal phalanx of the index finger to represent the index coordinate, while the other three markers (B_o, B_x, and B_y) attached at the back side of the hand were used to represent the body frame. With this marker configuration, $I^z_{I,B}$, which is a z-axis of the index coordinate represented in the body frame, was calculated. Also, we defined the amount of the robot's torsional shift at the i^{th} repeated motion as

$$\theta^i_{tilt} = \angle(I^{z,i+1}_{I,B}, I^{z,1}_{I,B}), \quad i = 1,2,...,25 \tag{S14}$$

where, $I^{z,i+1}_{I,B}$ is $I^z_{I,B}$ measured at the i^{th} extended posture; similarly, $I^{z,1}_{I,B}$ is $I^z_{I,B}$ measured at the initial posture.

D.2 Experimental protocol for experiment 2

Experiment 2 was conducted to validate whether the Exo-Glove Shell can assist three primitive motions with four actuators. In this experiment, a motion capture system was used to measure the joint angle of the thumb, index, and middle finger using a total of 16 markers, as shown in Fig. S10(b). 8 markers (I_0 - I_3 and M_0 - M_3) were attached to each of the index and middle finger (four for each finger) and five markers (T_i, T_j, T_o, T_1, and T_2) were attached to the thumb. Also, to find out the body frame, three markers were attached to the backside of the hand to define the body frame. Using these marker configurations, three indicators for the DOF analysis were defined as

$$
\begin{aligned}
Q_{TABD} &= q_{CMC.ABD} \\
Q_{TFE} &= mean(q_{CMC.FE}, q_{MCP.FE}, q_{IP.FE}) \\
Q_{MIFE} &= mean(q_{I.FE}, q_{M.FE})
\end{aligned}
\tag{S15}
$$

where, $q_{joint,direction}$ is the joint angle in specific direction - e.g., $q_{CMC.ABD}$ means the joint angle of the CMC joint in the abduction/adduction direction. I and M means joints of index and middle finger, respectively. For the thumb CMC joint, the $XY'Z''$ Euler angle was used to measure the three-directional motion using three markers (T_o, T_i and T_j); X-axis (*Unit* $[T_0 - T_j]$) represents the rotational axis related to the flexion/extension, Y-axis (*Cross* [Z-axis, X-axis]) represents the axis related to the abduction/adduction and Z-axis (*Unit* $[T_0 - T_i]$) represents the supination/pronation [31]; the *Unit* operator represents the normalized vector of the vector inside the bracket, while the *Cross* operator is used to represent the cross product. For the other joints, since these joints show only one DOF motion, the joint angle was obtained using a dot product of two phalange vectors. Q_{TABD}, Q_{TFE}, and Q_{MIFE} were obtained when assisting the thumb abduction/adduction motion, the thumb flexion/extension motion, and the middle/index finger flexion/extension motion. We obtained the joint angle data while assisting through five repeated motions.

D.3 Experimental protocol for experiment 3

The Exo-Glove Shell assists users with grasping in daily activities by dividing the grasp procedure into pre-grasp and actual grasp stages. In these two stages, the robot operates under different control methods, as follows: 1) position control in the pre-grasp phase; and 2) force control in the actual grasp phase. In the pre-grasp phase, the robot aims to prepare the posture in which the thumb is properly positioned relative to the other fingers to grasp objects stably. In the actual grasp phase, the robot is controlled to apply sufficient force to the objects. Experiment 3 shows how the robot assists with both a power grasp and a lateral pinch grasp.

In the pre-grasp phase during the power grasp assistance, we measured the thumb height (h_{thumb}) and orientation angle (C_{thumb}) in the index coordinates, which were defined as

$$
\begin{aligned}
h_{thumb} &= O^z_{T,IF} \\
C_{thumb} &= \angle(\hat{Z}_{IF}, \hat{Z}_T)
\end{aligned}
\tag{S16}
$$

where, $O^z_{T,IF}$ is the z-directional value represented in the index frame; $\hat{Z}_{IF}$ and $\hat{Z}_T$ is the z-axis of the index finger and the thumb represented in the global frame. These variables are represented in Fig. 6(a) of the main text.

A total of nine markers were used to measure the hand motion, as shown in Fig. S10(c); three markers with L-shaped structures were attached to the tips of the index and thumb, respectively, to define the index and thumb coordinates. The remaining three markers (B_o, B_i, and B_j) were used to define the body frame. By defining a transformation matrix between the thumb coordinate and the index coordinate, it was possible to obtain the z-axis ($O^z_{T,IF}$) of the thumb origin described in the index coordinate.

In the lateral pinch grasp assistance, we aimed to position the thumb so that it could press the side of the index finger in the pre-grasp phase. In other words, when we rotate the thumb tip toward the index plane (with the center of rotation as a CMC joint), the tip should exist inside the workspace (which is assumed to be a 2D plane by ignoring the abduction/adduction motion of the index finger) of the index finger. Accordingly, we defined $P_{T,IF} \in \mathbb{R}^2$ as

$$
\begin{aligned}
P_{T,IF} &= [r_{norm} O^x_{T,IF}, r_{norm} O^y_{T,IF}] \\
r_{norm} &= L_{Thumb} / \|[O^x_{T,IF}, O^y_{T,IF}]\|
\end{aligned}
\tag{S17}
$$

where, $O^x_{T,IF}$ and $O^y_{T,IF}$ are the x-directional value and y-directional value of the thumb fingertip represented in the index coordinate, respectively. In this equation, r_{norm} is a normalization factor to make the length of $P_{T,IF}$ to be same as the length of the thumb (L_{Thumb}); $\|A\|$ means the size of vector A. Similar to the power grasp experiment, the 9 markers shown in Fig. S10(c) were used to define $P_{T,IF}$ in Eq (S17).

Table S4: Summary of subject description

Gender	Age	Injury region	Year occurred	Rehabilitation duration	Other features
Male	40	C5,6 (ASIA-A)	August, 2002	20 months	Unable to move all fingers but can feel pain

D.4 Experimental protocol for experiment 4

In hand-wearable robot studies, numerous methods have been proposed to measure the robot's performance in the force domain. One of the well-used methods is to validate the fingertip force to show the robot's performance. However, generating a fingertip force in a single contact point might be less important in practical grasping [41]. Instead, satisfying the force closure condition by increasing contact points with the object might be a way to increase the stability of the grasp. Therefore, if there are n number of contact points, the sum of the contact forces ($F_{c,i}$ in Eq (3) of the main text) can be an indicator of the grasp stability.

For this reason, we designed an experimental setup that estimates the sum of the contact force, as shown in Fig. 9(a) in the main text, similar to the previous study [11]. This setup also has the advantage of being able to measure the performance of the robot when grasping objects of various shapes with a single experimental setup. Using this experimental setup, we measured the grasp performance factor (P_{force}) in the force domain, as described in Eq (3) in the main text.

The experiments were conducted 5 times each, using a cylinder-shaped object and a card-shaped object, and the average value of P_{force} was used for the experiment. In the experiments, the objects grasped were made using a 3D printer. The friction coefficient (μ_k in Eq (3) in the main text) was measured by another experiment as 0.38. Further, to prevent any threat of injury, the vertical moving distance (d in Fig. 9(b) of the main text) of the object and the speed were set to 30mm and 10mm/s, respectively.

D.5 Qualitative assessment of the Exo-Glove Shell

When developing the wearable robot, it is also important to consider qualitative aspects of the robot because the robot is directly worn by the user. Therefore, we prepared and asked qualitative questions to the experimental participant (a single SCI person as shown in Table S4) after proceeding with the quantitative validations (Experiments 2 - 4). The experimental participant did not experience any severe spasticity during the experiment. Also, the participant's initial finger posture was straight, therefore, wearing the robot was not so difficult. Please check our interview video at https://youtu.be/2-DfdRhCtMY (or our publication website at https://sites.google.com/view/exo-gloveshell) for more information. The interview in the video is documented below.

The advantages of Exo-Glove Shell are:

1. Metal rings make the robot safe and reliable compared to other robots that don't use the rings. (The experimental participant has many experiences in wearable robot experiments conducted in our previous robots.)
2. The robot easily makes thumb motions by guiding the movement using the rigid guide (even though the thumb has many degrees of freedom).
3. I feel safe and hardly feel any pain when using the robot (He can sense the pain even though he cannot move the finger.)
4. It's light and it seems easy to wash.
5. The shell structure of the router may make the glove difficult to wear, but they actually make it easier to wear by maintaining the shape of the finger holes at the glove.
6. The weight of the metal ring is not that significant.
7. The robot assists the lateral pinch posture, which is the posture I have wanted the most.

We also asked the participant about how we could improve the robot. The answers from the experimental participant are

1. Although it is good to use, customization should be considered.
2. The method to operate the robot should be improved. For example, a GUI platform to let users operate the robot would be useful.

References

[1] P. N. Soucacos. Indications and selection for digital amputation and replantation. *Journal of Hand Surgery*, 26 B(6):572–581, 2001.

[2] Leonardo Cappello, Jan T Meyer, Kevin C Galloway, Jeffrey D Peisner, Rachael Granberry, Diana A Wagner, Sven Engelhardt, Sabrina Paganoni, and Conor J Walsh. Assisting hand function after spinal cord injury with a fabric-based soft robotic glove. *Journal of neuroengineering and rehabilitation*, 15(1):1–10, 2018.

[3] Youngmok Yun, Sarah Dancausse, Paria Esmatloo, Alfredo Serrato, Curtis A. Merring, Priyanshu Agarwal, and Ashish D. Deshpande. Maestro: An EMG-driven assistive hand exoskeleton for spinal cord injury patients. *Proceedings - IEEE International Conference on Robotics and Automation*, pages 2904–2910, 2017.

[4] Paria Esmatloo and Ashish D. Deshpande. Fingertip position and force control for dexterous manipulation through model-based control of hand-exoskeleton-environment. *IEEE/ASME International Conference on Advanced Intelligent Mechatronics, AIM*, 2020-July(June):994–1001, 2020.

[5] Marco Cempini, Alberto Marzegan, Marco Rabuffetti, Mario Cortese, Nicola Vitiello, and Maurizio Ferrarin. Analysis of relative displacement between the HX wearable robotic exoskeleton and the user's hand. *Journal of NeuroEngineering and Rehabilitation*, 11(1), 2014.

[6] Ciarán O'Neill, Tommaso Proietti, Kristin Nuckols, Megan E Clarke, Cameron J Hohimer, Alison Cloutier, David J Lin, and Conor J Walsh. Inflatable soft wearable robot for reducing therapist fatigue during upper extremity rehabilitation in severe stroke. *IEEE Robotics and Automation Letters*, 5(3):3899–3906, 2020.

[7] Panagiotis Polygerinos, Kevin C Galloway, Emily Savage, Maxwell Herman, Kathleen O'Donnell, and Conor J Walsh. Soft robotic glove for hand rehabilitation and task specific training. In *2015 IEEE international conference on robotics and automation (ICRA)*, pages 2913–2919. IEEE, 2015.

[8] Mengli Sui, Yiming Ouyang, Hu Jin, Zhenyi Chai, Changyang Wei, Jiyu Li, Min Xu, Weihua Li, Liu Wang, and Shiwu Zhang. A soft-packaged and portable rehabilitation glove capable of closed-loop fine motor skills. *Nature Machine Intelligence*, pages 1–12, 2023.

[9] Phillip Tran, Seokhwan Jeong, Steven L Wolf, and Jaydev P Desai. Patient-specific, voice-controlled, robotic flexotendon glove-ii system for spinal cord injury. *IEEE Robotics and Automation Letters*, 5(2):898–905, 2020.

[10] Dong Hyun Kim, Yechan Lee, and Hyung-Soon Park. Bioinspired High-Degrees of Freedom Soft Robotic Glove for Restoring Versatile and Comfortable Manipulation. *Soft Robotics*, 00(00):1–11, 2021.

[11] Brian Byunghyun Kang, Hyungmin Choi, Haemin Lee, and Kyu Jin Cho. Exo-Glove Poly II: A Polymer-Based Soft Wearable Robot for the Hand with a Tendon-Driven Actuation System. *Soft Robotics*, 6(2):214–227, 2019.

[12] Michele Xiloyannis, Ryan Alicea, Anna-Maria Georgarakis, Florian L Haufe, Peter Wolf, Lorenzo Masia, and Robert Riener. Soft robotic suits: State of the art, core technologies, and open challenges. *IEEE Transactions on Robotics*, 38(3):1343–1362, 2021.

[13] Phillip Tran, Seokhwan Jeong, Kinsey R. Herrin, and Jaydev P. Desai. Review: Hand Exoskeleton Systems, Clinical Rehabilitation Practices, and Future Prospects. *IEEE Transactions on Medical Robotics and Bionics*, 3(3):606–622, 2021.

[14] Hyunki In, Brian Byunghyun Kang, Minki Sin, and Kyu-Jin Cho. Exo-glove: A wearable robot for the hand with a soft tendon routing system. *IEEE Robotics & Automation Magazine*, 22(1):97–105, 2015.

[15] Phillip Tran, Seokhwan Jeong, Steven L Wolf, and Jaydev P Desai. FLEXotendon Glove-II System for Spinal Cord Injury. *IEEE Robotics and Automation Letters*, 5(2):898–905, 2020.

[16] Dong Hyun Kim, Si Hwan Heo, and Hyung Soon Park. Biomimetic finger extension mechanism for soft wearable hand rehabilitation devices. *IEEE International Conference on Rehabilitation Robotics*, pages 1326–1330, 2017.

[17] Dong Hyun Kim and Hyung Soon Park. Cable Actuated Dexterous (CADEX) Glove for Effective Rehabilitation of the Hand for Patients with Neurological diseases. *IEEE International Conference on Intelligent Robots and Systems*, pages 2305–2310, 2018.

[18] Alireza Mohammadi, Jim Lavranos, Peter Choong, and Denny Oetomo. Flexo-glove: A 3D Printed Soft Exoskeleton Robotic Glove for Impaired Hand Rehabilitation and Assistance. *Proceedings of the Annual International Conference of the IEEE Engineering in Medicine and Biology Society, EMBS*, 2018-July:2120–2123, 2018.

[19] Hyunki In, Useok Jeong, Haemin Lee, and Kyu Jin Cho. A Novel Slack-Enabling Tendon Drive That Improves Efficiency, Size, and Safety in Soft Wearable Robots. *IEEE/ASME Transactions on Mechatronics*, 22(1):59–70, 2017.

[20] Wenyuan Chen, Guangyong Li, Ning Li, Wenxue Wang, Peng Yu, Ruiqian Wang, Xiujuan Xue, Xingang Zhao, and Lianqing Liu. Soft Exoskeleton With Fully Actuated Thumb Movements for Grasping Assistance. *Transactions on Robotics*, pages 1–14, 2022.

[21] Yong Jae Kim. Anthropomorphic low-inertia high-stiffness manipulator for high-speed safe interaction. *IEEE Transactions on Robotics*, 33(6):1358–1374, 2017.

[22] Ryuta Ozawa, Hiroaki Kobayashi, and Kazunori Hashirii. Analysis, classification, and design of tendon-driven mechanisms. *IEEE Transactions on Robotics*, 30(2):396–410, 2014.

[23] Byungchul Kim, Jiwon Ryu, and Kyu-jin Cho. Joint Angle Estimation of a Tendon-driven Soft Wearable Robot through a Tension and Stroke Measurement. *Sensors (Switzerland)*, pages 1–20, 2020.

[24] Ramana Vinjamuri. *Advances in motor neuroprostheses*. Springer, 2020.

[25] Michele Xiloyannis, Leonardo Cappello, Dinh Binh Khanh, Shih-Cheng Yen, and Lorenzo Masia. Modelling and design of a synergy-based actuator for a tendon-driven soft robotic glove. In *2016 6th IEEE International Conference on Biomedical Robotics and Biomechatronics (BioRob)*, pages 1213–1219. IEEE, 2016.

[26] Ryan Alicea, Michele Xiloyannis, Domenico Chiaradia, Michele Barsotti, Antonio Frisoli, and Lorenzo Masia. A soft, synergy-based robotic glove for grasping assistance. *Wearable Technologies*, 2:e4, 2021.

[27] Cosimo Della Santina, Cristina Piazza, Giorgio Grioli, Manuel G. Catalano, and Antonio Bicchi. Toward dexterous manipulation with augmented adaptive synergies: The pisa/iit softhand 2. *IEEE Transactions on Robotics*, 34(5):1141–1156, 2018.

[28] Yaohui Chen, Sing Le, Qiao Chu Tan, Oscar Lau, Fang Wan, and Chaoyang Song. A lobster-inspired robotic glove for hand rehabilitation. *Proceedings - IEEE International Conference on Robotics and Automation*, pages 4782–4787, 2017.

[29] Chad G. Rose and Marcia K. O'Malley. Hybrid Rigid-Soft Hand Exoskeleton to Assist Functional Dexterity. *IEEE Robotics and Automation Letters*, 4(1):73–80, 2019.

[30] Emanuel Todorov, Tom Erez, and Yuval Tassa. Mujoco: A physics engine for model-based control. In *2012 IEEE/RSJ international conference on intelligent robots and systems*, pages 5026–5033. IEEE, 2012.

[31] Zong Ming Li and Jie Tang. Coordination of thumb joints during opposition. *Journal of Biomechanics*, 40(3):502–510, 2007.

[32] Byungchul Kim, Useok Jeong, Brian Byunghyun Kang, and Kyu Jin Cho. Slider-Tendon Linear Actuator with Underactuation and Fast-connection for Soft Wearable Robots. *IEEE/ASME Transactions on Mechatronics*, 26(6):2932–2943, 2021.

[33] Minji Kim, Junyoung Park, Juhyeok Kim, Myungsin Kim, and Dongjun Lee. Stiffness Decomposition and Design Optimization of Under-Actuated Tendon-Driven Robotic Systems. *Proceedings - IEEE International Conference on Robotics and Automation*, pages 2266–2272, 2018.

[34] M. G. Catalano, G. Grioli, E. Farnioli, A. Serio, C. Piazza, and A. Bicchi. Adaptive synergies for the design and control of the Pisa/IIT SoftHand. *International Journal of Robotics Research*, 33(5):768–782, 2014.

[35] Li Chieh Kuo, Haw Yen Chiu, Cheung Wen Chang, Hsiu Yun Hsu, and Yun Nien Sun. Functional workspace for precision manipulation between thumb and fingers in normal hands. *Journal of Electromyography and Kinesiology*, 19(5):829–839, 2009.

[36] Tetsuya Mouri. Anthropomorphic Robot Hand: Gifu Hand III. *Iccas2002*, page 174, 1981.

[37] Dong Hyuk Lee, Jae Han Park, Sung Woo Park, Moon Hong Baeg, and Ji Hun Bae. KITECH-Hand: A Highly Dexterous and Modularized Robotic Hand. *IEEE/ASME Transactions on Mechatronics*, 22(2):876–887, 2017.

[38] Griffin Weston B, Findley Ryan P, Turner Michael L, and Cutkosky Mark R. Calibration and Mapping of a Human Hand for Dexterous Telemanipulation. In *Haptic Interfaces for Virtual Environments and Teleoperator Systems Symposium*, pages 1 – 8, 2000.

[39] Malvezz Monica, Gioioso Guido, Salvietti Gionata, and Prattichizzo Domenico. SynGrasp: A MATLAB Toolbox for Underactuated and Compliant Hands. *IEEE Robotics and Automation Magazine*, 2015.

[40] Marco Santello, Martha Flanders, and John F. Soechting. Postural hand synergies for tool use. *Journal of Neuroscience*, 18(23):10105–10115, 1998.

[41] Kevin M. Lynch and Frank C. Park. *Introduction To Modern Robotics Mechanics, Planning, and Control*. Cambridge University Press, 2016.